Available online at www.sciencedirect.com
ScienceDirect
Journal of Magnetic Resonance 184 (2007) 275–291
JMR Journal of Magnetic Resonance
www.elsevier.com/locate/jmr

Dynamics of paramagnetic agents by off-resonance rotating frame technique in the presence of magnetization transfer effect

Huiming Zhang [a,b,*], Yang Xie [a]

[a] Center for Basic MR Research, Evanston Northwestern Healthcare Research Institute, 1033 University Place, suite 100, Evanston, IL 60201, USA
[b] Department of Radiology, Feinberg Medical School of Northwestern University, Chicago, IL 60611, USA

Received 18 August 2006; revised 6 November 2006
Available online 22 November 2006

Abstract

The simple method for measuring the rotational correlation time of paramagnetic ion chelates via off-resonance rotating frame technique is challenged *in vivo* by the magnetization transfer effect. A theoretical model for the spin relaxation of water protons in the presence of paramagnetic ion chelates and magnetization transfer effect is described. This model considers the competitive relaxations of water protons by the paramagnetic relaxation pathway and the magnetization transfer pathway. The influence of magnetization transfer on the total residual z-magnetization has been quantitatively evaluated in the context of the magnetization map and various difference magnetization profiles for the macromolecule conjugated Gd-DTPA in cross-linked protein gels. The numerical simulations and experimental validations confirm that the rotational correlation time for the paramagnetic ion chelates can be measured even in the presence of strong magnetization transfer. This spin relaxation model also provides novel approaches to enhance the detection sensitivity for paramagnetic labeling by suppressing the spin relaxations caused by the magnetization transfer. The inclusion of the magnetization transfer effect allows us to use the magnetization map as a simulation tool to design efficient paramagnetic labeling targeting at specific tissues, to design experiments running at low RF power depositions, and to optimize the sensitivity for detecting paramagnetic labeling. Thus, the presented method will be a very useful tool for the *in vivo* applications such as molecular imaging via paramagnetic labeling.

Keywords: Off-resonance rotating frame; Paramagnetic relaxation enhancement; Magnetization transfer effect; Magnetization map; Magnetization profiles; Difference magnetization profiles; Dynamic of paramagnetic ion chelates

1. Introduction

Paramagnetic labeling permits to image the specific process in molecular/cellular events non-invasively by MRI. The dynamic parameters such as the motional correlation time of the labeling can be an important marker to highlight the binding processes of labeled ligands to targets. Traditionally, the dynamics of paramagnetic agents are extracted from the field dependent relaxivity using a specific spectrometer called field cycling spectrometer that sweeps from 0.01 kHz to 30 MHz at proton Larmor frequency [1,2]. Recently, we have demonstrated a novel method to determine the rotational correlation time of paramagnetic ion chelates with single magnetic field. This method is established on the basis of paramagnetic relaxation enhancement in off-resonance rotating frame at the magnetic field strength higher than 3T [3,4]. With the guidance of a simulation tool called magnetization map [4], the residual z-magnetization profiles are acquired in such way that their characteristics are directly correlated with the rotational correlation time. Three types of difference magnetization profiles are generated from the residual z-magnetization profiles. By comparing these profiles with the standards, the rotational correlation time of the paramagnetic ion chelates can be identified. Because the paramagnetic relaxation enhancement efficiency is proportional to $(\omega_H \tau_R)^2$, this method can effectively differentiate the

* Corresponding author. Fax: +1 847 492 0731.
E-mail address: h-zhang1@northwestern.edu (H. Zhang).

1090-7807/$ - see front matter © 2006 Elsevier Inc. All rights reserved.
doi:10.1016/j.jmr.2006.11.004

rotational correlation time for the *in vivo* applications at high magnetic fields.

However, the off-resonance rotating frame is achieved by the long off-resonance pulse as shown in the previous paper [3], which is the same routine sequence used in NMR/MRI for the spin saturations or magnetization transfer (MT) [5,6], and for the spin relaxations in the off-resonance rotating frame [7–11]. One of the challenges for the *in vivo* applications is the interference of magnetization transfer effect [6], which is the dominant relaxation mechanism for the proton spins in tissues under the off-resonance irradiations. Since the paramagnetic ion chelates can relax water proton at much faster time scale than the magnetization transfer, the contribution of magnetization transfer effect is considered only for the pulse duration (<0.5 s) that is much shorter than that for reaching the steady state (a few seconds). Although applying short RF irradiations can reduce the contribution from the magnetization transfer, there are four important issues needed to be addressed for the *in vivo* applications. (1) What is the spin relaxation mechanism for water protons in the presence of paramagnetic agents and magnetization transfer? (2) What is the effect of magnetization transfer on the magnetization map of paramagnetic agents as a function of rotational correlation time? (3) What is the effect of magnetization transfer on the difference magnetization profiles of paramagnetic agents as a function of rotational correlation time? (4) How to suppress the magnetization transfer? To address these issues, we need a method to generate the transient residual z-magnetization for the magnetization transfer effect and a spin relaxation model for water protons in the presence of paramagnetic agents and magnetization transfer effect.

Magnetization transfer in a magnetic resonance imaging context was introduced by Wolff in 1989, who used the off-resonance irradiations to selectively detect the protons with different mobility that are coupled together via chemical exchange or through space dipolar interactions [6]. The mechanism of the spin coupling is described traditionally by a two-pool model for the protons of different mobility: the free water is denoted as the liquid pool and the water bound to the biopolymers is denoted as the semi-rigid pool [12,13]. Several groups have considered a three-pool model by further dividing the liquid pool into two pools: one for the free water and the other for the mobile biopolymers [14,15]. The comprehensive reviews on the methodology of magnetization transfer can be found elsewhere [12,13]. Here we only present those approaches that are relevant to the derivation of the formalism in this paper. Among the quantitative interpretations based on the two-pool model, Henkelman's approach permits to calculate the residual z-magnetization profiles in a simple way [16,17]. The formalism uses six parameters to calculate the steady state magnetization M_s at pulse duration $\tau \to \infty$ and most of them can be measured experimentally. This model has been used to simulate the residual z-magnetization profiles for Agar gels [17,18], where a lineshape function such as Lorentzian, Gaussian, super-Lorentzian or flexible function was used to describe the distribution of the spin–spin relaxation rate constant in the semi-rigid pool. Among these lineshape functions, only the Lorentzian and Gaussian have the simple analytical expressions, the other two lineshape functions were used to fit experimental data via numerical simulations. The transient residual z-magnetization for the liquid pool at an arbitrary pulse duration τ was derived as a single exponential function $M(\tau) = A\exp(-R_{app}\tau) + B$ [19,20], and as a multi-exponential function $M(\tau) = Ae^{-a\tau} + Be^{-b\tau} + Ce^{-c\tau}\cos(s\tau) + D/se^{-c\tau}\sin(s\tau) + E$ [21,22]. But these analytical expressions do not contain any lineshape function for the semi-rigid pool. The effect of short pulse delay (TR) can be included in the formalism by using $M(\mathrm{TR}) = M_s(1 - \exp(-\mathrm{TR}/T_1)$ [12,23]. Sled etc. have included the effect of the super-Lorentzian lineshape function in the transient magnetizations for gradient spoiled MRI by adding a fifth differential equation in the coupled magnetization equations, which provides a numerical approach to simulate the effect of transient magnetization transfer [24]. Gadolinium contrast agents have been used to shorten the T_1 for clinic applications, which also causes the reduction of magnetization transfer [25–27]. The theoretical understanding for this reduction is limited to the replacement of a shorter T_1 for the liquid pool. The analysis has been reported for the measurement at magnetic fields lower than 2 Tesla [28,29].

The system we considered here is a situation in which the paramagnetic relaxation pathway and magnetization transfer pathway coexist. In order to extract the information for the paramagnetic relaxation pathway, the off-resonance irradiations are selected at the RF conditions that can generate efficient paramagnetic relaxation enhancement. The typical experiments are set at $\omega_1 \geqslant 2$ kHz with pulse duration ranges from 25 ms to 500 ms, as we have shown in the previous paper [3,4]. Although there is a numerical simulation method to assess the residual z-magnetization profiles for the magnetization transfer effect [24], an analytical formalism approach will permit to directly examine the relations between various parameters. Based on the assumption of single exponential function, we propose a simple equation for calculating the residual z-magnetization by including the steady state magnetization M_s, and introduce an experimentally measurable parameter, the apparent relaxation rate constant R_{MT} in the rotating frame. This equation permits to evaluate the transient residual z-magnetization caused by the magnetization transfer for various biological systems.

To explore the effect of magnetization transfer on the relaxation enhancement of paramagnetic agents experimentally, we have used paramagnetic ion chelates trapped in gels to generate a system in which both paramagnetic relaxation and magnetization transfer effect exist. We have chosen the cross-linked bovine albumin (BSA) as the gel, which has been extensively used as tissue models in MRI [30]. Its parameters for simulating the steady state magnetization M_s can be found elsewhere [14,29]. This system has

intense magnetization transfer effect with M_s as low as 0.1 [14]. The typical M_s for tissue/organs ranges from 0.95 to 0.2 [12], the smaller M_s normally represents the larger magnetization transfer effect. Using paramagnetic ion chelates in BSA gels permits us to quantify the magnetization transfer theoretically and verify them experimentally. In order to demonstrate the change in the gel media with respect to the aqueous media reported in the previous paper [4], the same macromolecules conjugated Gd-DTPA are used in this study, which are the $(Gd\text{-}DTPA)_8$-Dextran and $(Gd\text{-}DTPA)_{41}$-PAMAM-g5. In the gels, in additional to the magnetization transfer effect, the diffusion coefficient of water molecules will decrease from $\sim 2\times 10^{-5}\,cm^2$ to $\sim 5\times 10^{-6}\,cm^2$ and the motional correlation time of the paramagnetic ion chelates will increase. Both will alter the rotating frame relaxation rate constant and the relaxation enhancement efficiency, as predicted by the relaxation theory [3,4].

In this work, we present a spin relaxation model for water protons in the presence of paramagnetic ion chelates and magnetization transfer effect, which is further validated experimentally by examining Gd-DO3A in 10% BSA gels later. Based on this spin relaxation model, we expand the method described in the previous paper [4] for extracting the rotational correlation time of paramagnetic ion chelates in the presence of magnetization transfer effect. Starting with a theoretical model, the formalism for calculating the total residual z-magnetization is derived by including the contributions from the paramagnetic relaxation pathway and the magnetization transfer pathway. An analytical expression for the transient z-residual magnetization is derived for the magnetization transfer pathway, which contains the formalism for the steady state magnetization M_s obtained by Henkelman [16]. The transient z-residual magnetization is further converted into a function of effective field angle θ so that the influence of the magnetization transfer can be included in the magnetization map. Thus, the magnetization map can be used as a simulation tool for the paramagnetic ion chelates in the presence of magnetization transfer effect. In the similar way as in the previous paper [4], the magnetization map and the difference of magnetization profiles are correlated with the rotational correlation time τ_R of Gd-DTPA through the numerical simulations, which are further validated by the experimental data for the macromolecule conjugated Gd-DTPA in 7% cross-linked BSA gel. A new type of difference magnetization profiles based on the suppression of magnetization transfer are explored with the theoretical simulation and validated with the experimental data. The inclusion of the magnetization transfer effect allows us to use the magnetization map as a simulation tool to design efficient paramagnetic labeling targeting at specific tissues, to design experiments running at low RF power depositions, and to optimize the sensitivity for detecting paramagnetic labeling. Thus, the presented method will be a very useful tool for *in vivo* applications such as molecular imaging via paramagnetic labeling.

2. Method

2.1. Theoretical model

For the cross-linked protein gels containing paramagnetic ion chelates in the region of $(R_{1,1\rho})_{diamag} \ll (R_{1,1\rho})_{paramag}$, where $(R_{1,1\rho})_{diamag}$ and $(R_{1,1\rho})_{paramag}$ is the rotating frame relaxation rate constant for the diamagnetic contribution and the paramagnetic contribution, respectively, we consider the transient response of proton spins in the liquid pool to the off-resonance long pulse. Assuming the paramagnetic ion chelates are not bound to the protein gels, there are two relaxation pathways for the proton spins in the liquid pool. As described in the schematics of Fig. 1, one is the paramagnetic relaxation with the rate constant denoted as $R_{1\rho,Gd}$ in the off-resonance rotating frame; the other is the magnetization transfer with the rate constant denoted as R_{MT}, representing the apparent relaxation rate constant for the protons in the liquid pool that is in chemical exchanging or magnetization transferring with the protons in the semi-rigid pool. Microscopically, the protons in the liquid pool are primarily relaxed by any relaxation center that approximates to them, either the paramagnetic ion chelates or the semi-rigid proton lattice. At the condition that the pulse delay TR is much longer than the pulse duration τ, $TR \gg \tau$, the spins relaxed by the paramagnetic ion and the spins relaxed by the semi-rigid pool are considered as uncoupled. The rational for this assumption is based on three facts: (1) the effective distance for spins relaxed by the paramagnetic ions are as short as a few nm [3]; (2) both relaxation pathways originate from independent chemical/magnetization exchange processes; (3) the water bound to the paramagnetic ion has much faster chemical exchange rate than those bound to the semi-rigid pool. Since paramagnetic agents are uniformly distributed in the gel media, water in the liquid pool has equal chance to exchange with either relaxation centers. The population for each pathway

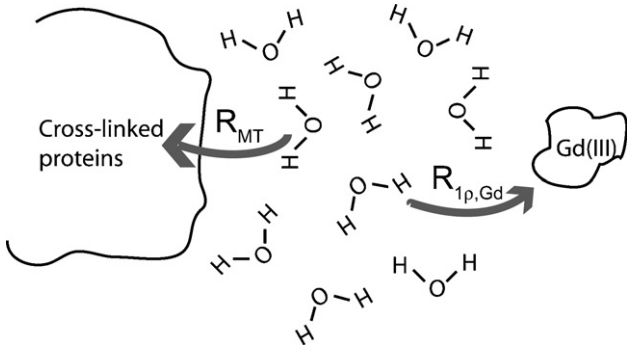

Fig. 1. Schematic illustration of the spin relaxation pathway for water proton in the presence of magnetization transfer effect and paramagnetic ion chelates. R_{MT} denotes the apparent relaxation rate constant for the magnetization transfer effect in the off-resonance rotating frame, $R_{1\rho,Gd}$ denotes the off-resonance rotating frame relaxation rate constant for the paramagnetic ion (Gd(III)) chelates.

depends on their relaxation rate constant, $R_{1\rho,\mathrm{Gd}}$ and R_{MT}. Thus, the spin relaxations for the liquid pool in the limit of $\mathrm{TR} \gg \tau$ can be considered as the sum of two independent relaxation processes and the rate constant for each pathway determines the contribution. Based on this physical picture as shown in Fig. 1, the total transient residual z-magnetization $M_e(\theta,\tau)$ can be described as follows:

$$M_e(\theta,\tau) = p_{\mathrm{Gd}} M_{\mathrm{Gd}}(\theta,\tau) + p_{\mathrm{MT}} M_{\mathrm{MT}}(\theta,\tau) \quad (1)$$

where θ is the effective field angle in the off-resonance rotating frame, $\theta = tg^{-1}(\omega_1/\Delta)$, in which ω_1 is the RF amplitude and Δ is the frequency offset. $M_{\mathrm{Gd}}(\theta,\tau)$ and $M_{\mathrm{MT}}(\theta,\tau)$ are the magnetization for the paramagnetic relaxation pathway and the magnetization transfer pathway, respectively. Their analytical expressions will be provided below. p_{Gd} is the contribution fraction for the paramagnetic relaxation pathway and p_{MT} is the contribution fraction for the magnetization transfer pathway, expressed as follows,

$$p_{\mathrm{Gd}} = R_{1\rho,\mathrm{Gd}}(\theta)/(R_{1\rho,\mathrm{Gd}}(\theta) + R_{\mathrm{MT}}) \quad (2)$$

$$p_{\mathrm{MT}} = 1 - p_{\mathrm{Gd}} \quad (3)$$

where $R_{1\rho,\mathrm{Gd}}(\theta)$ is the rotating frame relaxation rate constant for the paramagnetic ion chelates, its formalism is provided in the Appendix A, the apparent relaxation rate constant R_{MT} is an empirical parameter to characterize the spin relaxation rate of magnetization transfer under the long pulse and will be discussed later in details in Section 2.3.

Eq. (1) states that the total residual z-magnetization yields from the competitive relaxations of two pathways. In the limit of $R_{1\rho,\mathrm{Gd}}(\theta) \gg R_{\mathrm{MT}}$, where either the magnetization transfer relaxation rate constant R_{MT} is small or the paramagnetic relaxation rate constant $R_{1\rho,\mathrm{Gd}}(\theta)$ is very large, the contribution from the magnetization transfer pathway can be neglected completely. R_{MT} is determined by the tissues of various anatomy/physiology *in vivo*, but $R_{1\rho,\mathrm{Gd}}(\theta)$ can be increased by numerous ways [3,4]. Thus, dynamics of paramagnetic ion chelates in various biological systems can be extracted *in vivo*. However, if the condition $\mathrm{TR} \gg \tau$ is not satisfied, the spins of metal ion bound water and the spins of semi-rigid pool may be forced to couple together. In this case, Eq. (1) may not be validated anymore.

Eq. (1) naturally fits the physical model shown in Fig. 1. The dynamic features of this equation are generalized in details in Section 2.4. The method can be easily used for signal editing, parameters extraction and experimental designing as shown below. However, the question is if there is alternative analytical description for the spin relaxation model? One would think if the equation can be simplified by either replacing the relaxation rate constant for the proton in the liquid pool with the relaxation enhanced rate constant $R_{1\rho,\mathrm{Gd}}$ in the well-known coupled equation for the magnetization transfer model [19–21], or simply adding a factor to the $R_{1\rho,\mathrm{Gd}}$ to reflect the effect of magnetization transfer on the paramagnetic relaxation enhancement. The first approach is not appropriate; because it assumes that liquid pool is in equilibrium with the paramagnetic relaxation and neglects the fact that paramagnetic enhancement also affects the semi-rigid pool via the chemical exchange of water. The water in liquid pool actually in exchange with two sources, the semi-rigid pool and the paramagnetic relaxation center, each has its own exchange rate constant. The substitution of relaxation rate constant sets the water in liquid pool with the wrong exchange rate constant. The second approach may be worth to considerate if the extraction for the dynamics parameters can be assessed with a simple mathematic model.

2.2. Paramagnetic relaxation pathway

The transient residual z-magnetization for the paramagnetic relaxation pathway has been derived in the previous paper [4], which is expressed as follows:

$$M_{\mathrm{Gd}}(\theta,\tau) = M_0 \cos^2\theta[(1 - R_{1,\mathrm{Gd}}/R_{1\rho,\mathrm{Gd}}(\theta)) \times \exp(-R_{1\rho,\mathrm{Gd}}(\theta)\tau) + R_{1,\mathrm{Gd}}/R_{1\rho,\mathrm{Gd}}(\theta)] \quad (4)$$

with

$$R_{1,\mathrm{Gd}} = R^{\mathrm{IS}}_{1,\mathrm{Gd}} + sR^{\mathrm{OS}}_{1,\mathrm{Gd}} \quad (5)$$

$$R_{1\rho,\mathrm{Gd}}(\theta) = R^{\mathrm{IS}}_{1\rho,\mathrm{Gd}}(\theta) + sR^{\mathrm{OS}}_{1\rho,\mathrm{Gd}}(\theta) \quad (6)$$

where s is the space assessable coefficient for the outer shell water for the macromolecule conjugated paramagnetic ion chelates [3]. $R^{\mathrm{IS}}_{1,\mathrm{Gd}}$, $R^{\mathrm{OS}}_{1,\mathrm{Gd}}$ are the laboratory spin–lattice relaxation rate constants for the inner shell water (IS) and the outer shell water (OS), respectively. $R^{\mathrm{IS}}_{1\rho,\mathrm{Gd}}(\theta)$, $R^{\mathrm{OS}}_{1\rho,\mathrm{Gd}}(\theta)$ are the rotating frame spin–lattice relaxation rate constants; their formalisms are provided in the Appendix A. $R_{1,\mathrm{Gd}}$ and $R_{1\rho,\mathrm{Gd}}(\theta)$ are the total spin–lattice relaxation rate constants for the laboratory frame and the rotating frame, respectively. Using Eq. (4), we can calculate the magnetization map and various magnetization profiles for the paramagnetic relaxation pathway in the similar way the paramagnetic ion chelates in aqueous media [4].

Considering a short pulse delay TR is applied in the limit of $\mathrm{TR} \gg \tau$, TR can be included in the expression of the residual z-magnetization below,

$$M_{\mathrm{Gd}}(\theta,\tau,\mathrm{TR}) = M_{\mathrm{Gd}}(\theta,\tau)[1 - \exp(-R_{1,\mathrm{Gd}} \cdot \mathrm{TR})] \quad (7)$$

where $R_{1,\mathrm{Gd}}$ is the laboratory frame relaxation rate constant for the paramagnetic ion chelates. Because $R_{1,\mathrm{Gd}}$ is larger than the laboratory frame relaxation rate constant for the spins in the liquid pool, the use of short TR will benefit the paramagnetic relaxation pathway.

2.3. Magnetization transfer pathway

For the spin relaxations of magnetization transfer pathway, we assumed that the transient residual z-magnetization is a simple exponential function of pulse duration τ as follows:

$$M_{MT}(\theta,\tau) = A + B\exp(-R_{MT}\tau) \quad (8)$$

In this equation, R_{MT} defines the speed of the residual z-magnetization toward the equilibrium, A, B are the constants associated with the residual z-magnetization at equilibrium. Since most steady state magnetizations M_s are measured with the pulse duration as long as a few seconds, this RF condition is very close to the measurement of the residual z-magnetization at equilibrium in our study. Thus, the magnitude of M_s can be used as an approximation for the residual z-magnetization at equilibrium, which leads to $A = M_s$ and $B = M_0\cos^2\theta - M_s$. Note that R_{MT} is different from the exchange rate constant R in the spin coupling model of magnetization transfer. R is a rate constant depending on chemical structures of the exchangeable sites in the semi-rigid pool, the value ranges for tens to hundreds per second [16,17]. Much smaller than R, R_{MT} characterizes the decay rate of residual z-magnetization under the off-resonance irradiation, which may need as long as a few second to reach the equilibrium status. This R_{MT} is equivalent to the parameter k_{sat} used for the magnetization transfer effect in the literature. k_{sat} depends on the saturation scheme in general [13]. However, the saturation scheme in our experiment is uniquely defined as a hard pulse. Thus, the R_{MT} defined in this paper is a constant.

This assumption simplifies the complicated transient response for the magnetization transfer. Because R_{MT} is independent of θ angle, the dependence of $M_{MT}(\theta,\tau)$ on θ angle will be reflected through the coefficients A and B, both are a function of M_s. Here we use the formalism of M_s developed by Henkelman et al [16,17],

$$\begin{aligned} M_s = {} & M_0\{R_b[RM_0^b/R_a] + R_{rfb} + R + R_b\} \\ & /\{[RM_0^b/R_a](R_b + R_{rfb}) + (1 + (\omega_1/\Delta)^2) \\ & \times[1/R_aT_{2a}](R_b + R + R_{rfb})\} \end{aligned} \quad (9)$$

where $R_{a,b}$ is the spin–lattice relaxation rate constant for the liquid pool and the semi-solid pool, respectively, R is the exchange rate constant of the liquid pool (a) and the semi-solid pool (b), T_{2a} is the spin–spin relaxation rate constant for the liquid pool, RM_0^b is the pseudo-first-order rate constant for exchange from the liquid pool to the semi-solid pool, R_{rfb} is the spin–spin relaxation rate constant with specific lineshapes, $R_{rfb} = \omega_1^2\pi g_i(2\pi\Delta)$, where $g_i(2\pi\Delta)$ is a lineshape function. Here, the Lorentzian or Gaussian lineshape functions are used. The Gaussian lineshape $g_g(2\pi\Delta)$ fits well to the residual z-magnetization as a function of the frequency offset in logarithm scale for gels [16,17]. The formalism of $g_g(2\pi\Delta)$ is as follows:

$$g_g(2\pi\Delta) = \frac{T_2}{\sqrt{2\pi}}e^{-\frac{(2\pi\Delta T_2)^2}{2}} \quad (10)$$

and

$$R_{rfb(G)} = \sqrt{\frac{\pi}{2}}\omega_1^2 T_{2B}e^{-\frac{(2\pi\Delta T_2)^2}{2}}. \quad (11)$$

Thus, the residual z-magnetization for the magnetization transfer pathway as a function of frequency offset is as below

$$M_{MT}(\theta,\tau) = (M_0\cos^2\theta - M_{s(G)})\exp(-R_{MT}\tau) + M_{s(G)}. \quad (12)$$

where $M_{s(G)}$ is the residual z-magnetization at the steady state with the Gaussian lineshape function for R_{rfb}. The effect of TR can be included in the same way as that for the paramagnetic relaxation pathway as follows:

$$M_{MT}(\theta,\tau,TR) = M_{MT}(\theta,\tau)[1 - \exp(-R_a\cdot TR)] \quad (13)$$

The formalism of Gaussian lineshape function is not directly related to θ, which will make it difficult to correlate the lineshape function with the magnetization map. However, in the limit of $R_{rfb(g)} \gg R, R_b, R_b[RM_0^b/R_a]$, $M_{s(G)}$ can be simplified as a function of θ as follows:

$$M_{s(G)} = M_0\frac{1}{[RM_0^b/R_a] + (1 + tg(\theta)^2)[1/R_aT_{2a}]} \quad (14)$$

This limit depends primarily on the T_2 of the semi-rigid pool. For T_{2B} in tens of μs, Eq. (14) is valid at θ as low as 2°.

In order to obtain the θ-dependence that is valid for all θ angles, we consider the Lorentzian lineshape function $g_L(2\pi\Delta)$,

$$g_L(2\pi\Delta) = \frac{T_2}{\pi}\frac{1}{[1 + (2\pi\Delta T_2)^2]} \quad (15)$$

In the limit $2\pi\Delta T_{2B} \gg 1$ or the small θ angle, this lineshape function can be directly expressed as a function of θ angle as follows:

$$R_{rfB(L)} = \frac{T_{2B}\omega_1^2}{[1 + (2\pi\Delta T_{2B})^2]} \approx \frac{tg(\theta)^2}{T_{2B}} \quad (16)$$

Substitute Eq. (16) to Eq. (9), the residual z-magnetization at steady state $M_{s(L)}$ becomes,

$$\begin{aligned} M_{s(L)} = {} & M_0\left\{R_b[RM_0^b/R_a] + tg(\theta)^2/T_{2B} + R + R_b\right\} \\ & /\left\{[RM_0^b/R_a](R_b + tg(\theta)^2/T_{2B}) + (1 + tg(\theta)^2)\right. \\ & \left.\times[1/R_aT_{2a}](R_b + R + tg(\theta)^2/T_{2B})\right\} \end{aligned} \quad (17)$$

where the subscript L denotes for the Lorentzian lineshape.

Eq. (17) can be extended to the large θ angle for semi-rigid pools with T_{2B} in tens of μs. At this condition, $tg(\theta)^2/T_{2B} \gg R, R_b, R_b[RM_0^b/R_a]$, Eq. (17) can be simplified to Eq. (14). Thus, Eq. (17) can be used to generate θ dependent M_s for all θ angles. Therefore, the magnetization map for the magnetization transfer pathway can be generated by using the following equation to calculate the residual z-magnetization,

$$M_{MT}(\theta,\tau) = (M_0\cos^2\theta - M_{s(L)})\exp(-R_{MT}\tau) + M_{s(L)}. \quad (18)$$

In summary, steady state magnetization M_s with Lorentzian lineshape function for the semi-rigid pool can provide a direct dependence of θ angle and is suitable for generating magnetization map. For the semi-rigid pools with T_{2B} in tens of μs, $M_{s(L)}$ is different from $M_{s(G)}$ at θ less than a few degrees. However, this region is beyond the most sensitive region of paramagnetic relaxation enhancement ($\theta \sim 45°$). M_s in this region is expressed by Eq. (14), where $R_{rfb(g)} \gg R, R_b, R_b[RM_0^b/R_a]$. This condition can be used to explore the effect of the exchange rate constant on the magnetization map, as shown in Section 4.2 below.

2.4. Total residual z-magnetization

The total residual z-magnetization as a function of θ angle is the sum of the two relaxation pathways as follows:

$$\begin{aligned} M_e(\theta,\tau) = {} & p_{Gd}\{M_0\cos^2\theta[(1 - R_{1,Gd}/R_{1\rho,Gd}(\theta)) \\ & \times \exp(-R_{1\rho,Gd}(\theta)\tau) + R_{1,Gd}/R_{1\rho,Gd}(\theta)\} \\ & + p_{MT}\{(M_0\cos^2\theta - M_{s(L)})\exp(-R_{MT}\tau) + M_{s(L)}\} \end{aligned} \tag{19}$$

which permits to calculate the magnetization map for the protons in the liquid pool in the presence of the paramagnetic ion chelates and magnetization transfer effect.

Eq. (19) suggests that the total residual z-magnetization is a two-exponential function that can be generalized as $M(\tau) = A_1\exp(-k_1\tau) + A_2\exp(-k_2\tau) + (B_1 + B_2)$, where the subscript denotes the nth-pathway, A_i and B_i are the constant related to the initial and equilibrium/steady state magnetizations, k_i is the relaxation rate constant, $i = 1, 2$. In the limit of $k_i\tau \ll 1$, by using $\exp(x) \approx 1 - x$ relation, $M(\tau)$ can be simplified as a single exponential function as below

$$M(\tau) = (A_1 + A_2)\exp\left(-\frac{A_1k_1 + A_1k_2}{A_1 + A_2}\tau\right) + (B_1 + B_2) \tag{20}$$

This condition corresponds to the short τ or small relaxation rate constants, where $M(\tau)$ is a single exponential function that has the mixed contributions from two relaxation pathways. The separation of the relaxation information for the two pathways will be difficult. In the limit of $k_i\tau \gg 1$, $M(\tau) = B_1 + B_2$, which corresponds to the equilibrium/steady state. Since the total magnetization has the contribution from the paramagnetic relaxation pathway, its magnitude will be larger than that without the paramagnetic agents, as shown the reduction of magnetization transfer previously [25–27]. Between the two limits and with $k_1 > k_2$, the contribution of the slow relaxation component (the 2nd-component) can be reduced or eliminated by selecting appropriate τ. For $k_1\tau > 1$ and $k_2\tau \ll 1$, assuming $A_2[\exp(-k_2(\theta_1)\tau) - \exp(-k_2(\theta_2)\tau)] \sim 0$, the difference between $M(\tau)$ obtained at two RF conditions is directly related to the fast relaxation component as below

$$M(\theta_1,\tau) - M(\theta_2,\tau) \sim A_1[\exp(-k_1(\theta_1)\tau) - \exp(-k_1(\theta_2)\tau)] \tag{21}$$

Eq. (21) suggests the difference magnetization can be used to extract the relaxation parameters for the fast relaxation component. This has been the strategy for extracting the dynamic parameters of paramagnetic ion chelates in aqueous media [4], where no magnetization transfer effect exists. Thus, we can use the previous developed method to extract the dynamics of paramagnetic agents in the presence of magnetization transfer effect.

2.5. Numerical simulations

Calculations of residual z-magnetizations were performed for macromolecule conjugated Gd-DTPA in cross-linked protein gels. For Gd-DTPA, the parameters are the same as those used in previous paper [3,4]. They are $S = 7/2$, $q = 1$, $\tau_v = 38$ ps, $\tau_{s0} = 85$ ps, $\tau_m = 0.244$ μs, $r = 3.05$ Å, $\tau_R = 80$, 1500 and 3000 ps, $d = 3.6$ Å, $D = 5 \times 10^{-6}$ cm^2/s, $s = 0.75$, $c_{Gd} = 1$ or 10 mM. In this list, S is the electron spin number, q is the number of water molecular bound per metal ion, τ_v is the correlation time characterized the fluctuation of the zero field splitting (ZFS), τ_{S0} is related to ZFS constant B as $\tau_{S0} = \tau_v/5B$, τ_m is the residual time of structural water, r is the electron–proton distance, τ_R is the rotational correlation time, d is the distance of closest approach of the water molecule to the metal complex, D is the sum of the diffusion coefficients of water molecule (D_I) and metal ion complex (D_S), s is the space assessable coefficient for the outer shell water for macromolecule conjugated paramagnetic ions, c_{Gd} is the gadolinium concentration. RF amplitude ω_1 is 2, 4 and 6 kHz, and offset Δ varies from 5 kHz to 60 kHz. For protein gels, the parameters are $T_{1A} = 2.2$ s, $T_{1B} = 1$ s, $T_{2A} = 50$ ms, $T_{2B} = 12$ μs, $RM_0^B/R_A = 2$, $R = 2$ s^{-1}, $R_{MT} = 3.5$ s^{-1}, $R_{rfB} = 2\pi\omega_1^2 g_i(2\pi\Delta)$. The definition for these parameters can be found elsewhere [16], where subscripts A, B are denoted for the liquid pool and semi-rigid pool, $T_{1A,B}$ is the spin lattice relaxation time, $T_{2A,B}$ is spin–spin relaxation time, R is the exchange rate constant, RM_0^B is the pseudo-first-order rate constant (exchange from $A \rightarrow B$), $R_a = 1/T_{1A}$, and R_{MT} is the apparent relaxation rate constant for magnetization transfer. All calculations were performed with Mathematica software.

3. Experimental

3.1. Sample preparations

(Gd-DTPA)$_8$-Dextran and (Gd-DTPA-SCN-Bz)$_{41}$-PAMAM-g5 were synthesized as reported elsewhere [1]. Ligand 1,4,7,10-tetraazacyclododecane-1,4,7-tris-acetic acid (DO3A) from Macrocycles (Dallas, TX) was reacted with stoichiometric gadolinium (III) oxide to yield Gd-DO3A. Atomic emission spectroscopy (AES) was used to determine the concentration of the gadolinium in the final products. 7% and 10% bovine albumin (BSA) solution was cross-linked with 25% glutaraldehyde to form protein gels [31].

3.2. NMR measurements

All NMR experiments were carried with volume coils on a 9.4 T Bruker Avance micro-imaging spectrometer. Paramagnetic ion chelates at 1 mM Gd(III) in BSA gels were placed in a 5 mm tube in a Bruker ^{1}H 10 mm resonator at room temperature for the 9.4 T. The off-resonance rotating frame magnetization profiles were obtained by applying a long pulse with a 5–60 kHz frequency offset followed by a 90° reading pulse. The residual z-magnetization was plotted as a function of offset frequency to generate the magnetization profiles. Their fitted curves were used to generate the difference magnetization profiles. The off-resonance pulses were 500 ms long with RF amplitudes of 2, 4 and 6 kHz, the width of 90° pulse was 30 μs and the relaxation delay was 20 s.

4. Results and discussion

4.1. Contribution from each relaxation pathway

Fig. 2(A) shows the contribution fraction of the paramagnetic relaxation pathway p_{Gd} as a function of θ angle, which is calculated from the relaxation rate constant of the two pathways $R_{1\rho,Gd}(\theta)$ and R_{MT} by Eq. (2). Fig. 2(B) shows the relaxation rate constant ratio of $R_{1\rho,Gd}(\theta)/R_{MT}$ as a function of θ angle. These calculations are for the gadolinium chelates with one coordinated water ($q = 1$) at 1 mM Gd(III). A typical value of 5×10^{-6} cm^2/s is used for the water diffusion coefficient in the gel media [32,33]. R_{MT} is defined as 3.5 s^{-1} by comparing the theoretically calculated residual z-magnetization with the experimental measurement for 7% cross-linked BSA gels (data are not shown). Fig. 2(A) demonstrates the dependence of p_{Gd} on the rotational correlation time τ_R. For τ_R of 80 ps p_{Gd} is around 0.7, indicating that the paramagnetic relaxation pathway dominates the spin relaxation of the liquid pool. As τ_R increases from 1500 ps to 5000 ps, p_{Gd} is in the range of 0.8–0.98 at $\theta > 10°$. This arises from the dependence of $R_{1\rho,Gd}(\theta)/R_{MT}$ on τ_R, as shown in Fig. 2(B). $R_{1\rho,Gd}(\theta)/R_{MT}$ increases rapidly as τ_R increases at $\theta > 20°$ with the amplitude as high as ~50. Such large ratio provides dynamic range for the concentration of paramagnetic agents. The dose for paramagnetic agents can be reduced as long as $R_{1\rho,Gd}(\theta)/R_{MT}$ is sufficiently large. This result suggests that using the paramagnetic ion chelates with large τ_R can completely eliminate the interference of magnetization transfer at most θ angles (ω_1, Δ). In this ratio, $R_{1\rho,Gd}(\theta)$ also depends on the coordinated water number q and effective angle θ. Increase of q will increase $R_{1\rho,Gd}(\theta)$ by q-fold. For tissues with small apparent relaxation rate constant R_{MT}, the paramagnetic relaxation pathway can easily dominate the total relaxation of water spins.

4.2. Magnetization map for magnetization transfer effect

Fig. 3 shows the magnetization maps for the magnetization transfer effect with exchange rate constant $R = 2$, 100 by using Eq. (18). R for biological tissues has wide distributions [35,36]. $R = 2$ is close to the value reported for the cross-linked 10% BSA gels [14,29,34]; while $R = 100$ is relevant to the *in vivo* systems [35,36]. The Lorentzian lineshape is used to calculate R_{rfB}, which can provide accurate magnetization dependence of θ at small θ angle,

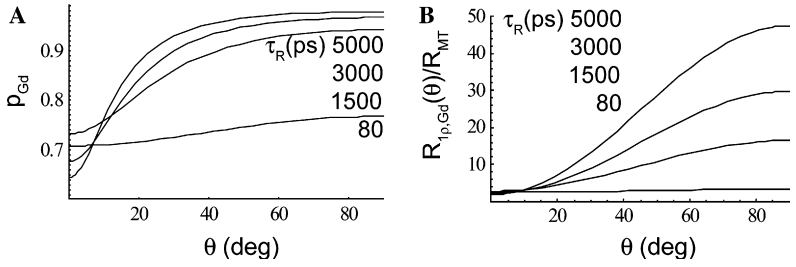

Fig. 2. Theoretically predicted contribution fraction of the paramagnetic relaxation pathway p_{Gd} (A) and the relaxation rate constant ratio of the two pathways $R_{1\rho,Gd}(\theta)/R_{MT}$ (B) at 9.4 T. Molecular parameters are discussed in the text.

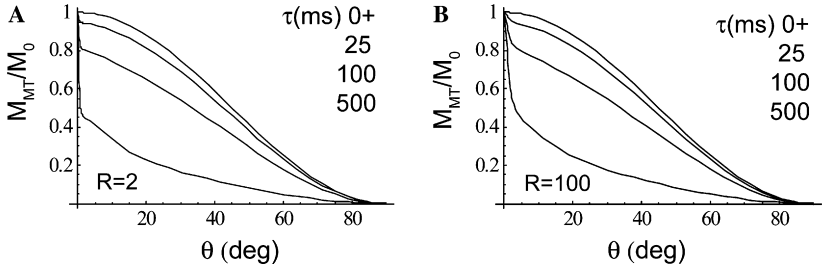

Fig. 3. Theoretically predicted magnetization map for cross-linked protein gels at 9.4 T with relaxation rate const exchange rate constant $R = 2$ (A) and $R = 100$ (B). Parameters used for simulation include $T_{1A} = 2.2$ s, $T_{1B} = 1$ s, $T_{2A} = 50$ ms, $T_{2B} = 12$ μs, $RM_0^B/R_A = 2$, $R_{MT} = 3.5$ and $R_{rfB} = 2\pi\omega_1^2 g_i(2\pi\Delta)$.

as discussed in Section 2.3. The apparent relaxation rate constant R_{MT} is 3.5 s^{-1} for the magnetization transfer pathway. In these calculations, the pulse duration τ is kept the same as that for the paramagnetic agents in the aqueous media [4] and assuming the pulse delay TR is sufficiently long. As θ increases, the residual z-magnetization decreases rapidly at short τ but slowly at long τ. The influence of this pathway on the total magnetization is determined by its contribution fraction p_{MT}, the apparent relaxation rate constant R_{MT} and the pulse delay TR. Among these parameters, TR is an experimental parameter and short TR reduces the residual z-magnetization. p_{MT} and R_{MT} are determined by the structure of tissues, but p_{MT} can be reduced by using paramagnetic ion chelates with high relaxation enhancement efficiency.

Fig. 4 shows the magnetization maps for the paramagnetic relaxation (the left panels), the total magnetization (the central panels) and the magnetization transfer portion (the right panels) at 9.4 T, which are calculated by using Eq. (4), Eq. (19) and the product of p_{MT} with Eq. (18), respectively. The magnetization maps are calculated for gadolinium chelates with one structural water ($q = 1$) at 1 mM Gd(III). The rotation correlation time τ_R is 80, 1500, 3000 and 5000 ps, respectively. The exchange rate constant R for the gels equals to 2. Comparing with the calculations in the aqueous media [4], the diffusion coefficient is reduced from 3.16×10^{-5} cm^2/s in the solutions to 5×10^{-6} cm^2/s in the gels. Along with this reduction, the following alterations are as expected. With the same τ_R, the dynamic range of the magnetization maps in the gels

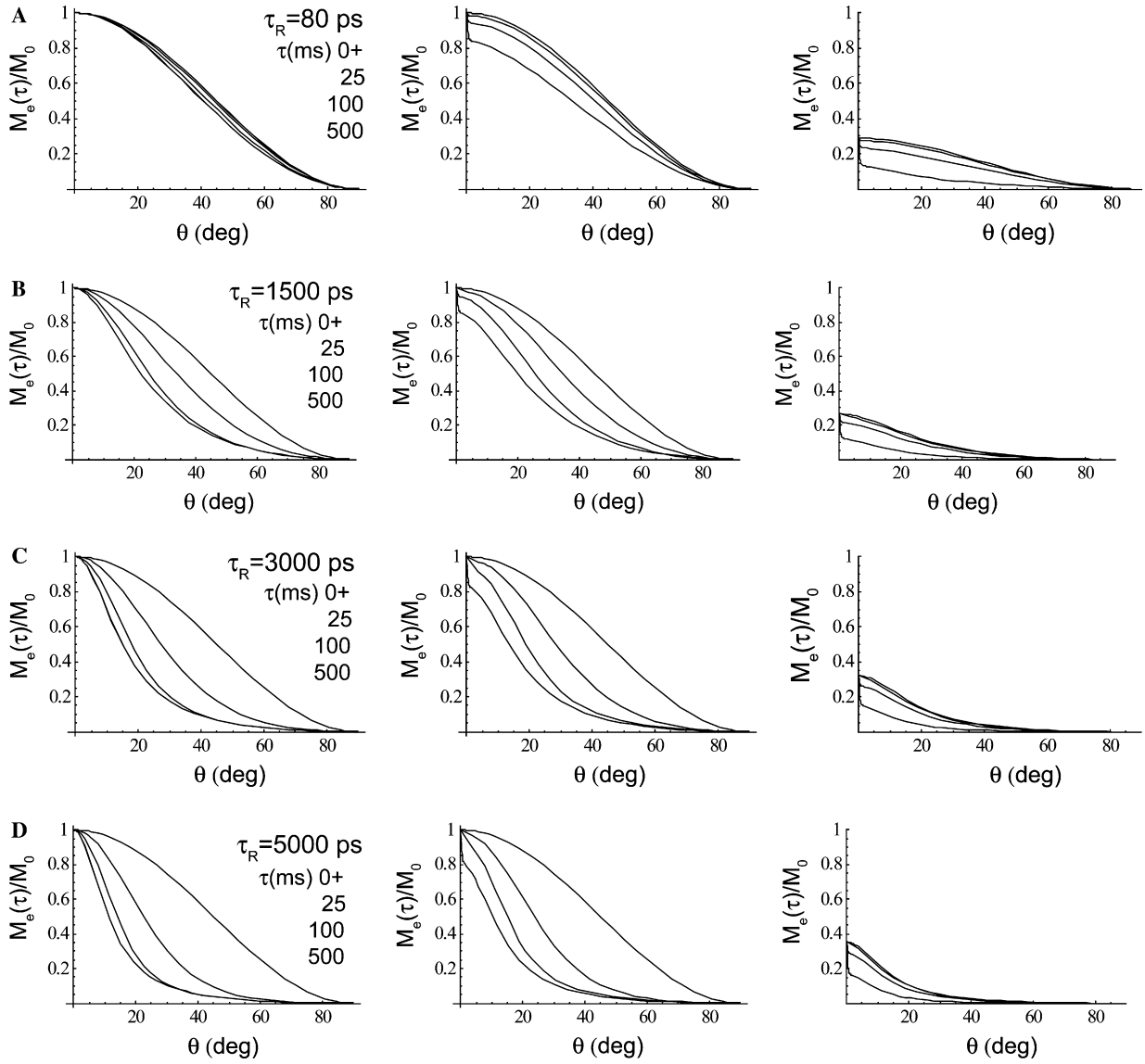

Fig. 4. Theoretically predicted magnetization map for gadolinium chelates in cross-linked protein gels at 9.4 T with $R = 2$. The left panels are the paramagnetic relaxation contribution with $p_{Gd} = 1$; the center panels are the total contribution from both relaxation pathways; and the right panels are the contribution from the magnetization transfer pathway. These maps are corresponding to the rotational correlation time τ_R of 80 ps (A), 1500 ps (B), 3000 ps (C) and 3000 ps (D). Molecular parameters are discussed in the text.

is much smaller than those in the aqueous media [4], which suggests the smaller relaxation enhancement efficiency $R_{1\rho,\mathrm{Gd}}(\theta)/R_{1,\mathrm{Gd}}$. The magnetization at $\tau = 100$ ms appears much closer to that at $\tau = 500$ ms, indicating a larger relaxation rate constant $R_{1\rho,\mathrm{Gd}}(\theta)$. For the magnetization transfer pathway, the large contributions are located at the small θ angle region with amplitude ranging from 0.2 to 0.3. For the total magnetization, the contribution of magnetization transfer alters the magnetization map. The region being distorted varies as a function of τ_R. For small τ_R of 80 ps, the magnetization map is distorted seriously. For large $\tau_R > 1500$ ps, most distortions occur at $\theta < 10°$. The region ($\theta \sim 45°$) that is most sensitive to the paramagnetic relaxation enhancement remains the same as that for the paramagnetic relaxation alone. This allows us to extract the rotational correlation time in the same way as that in aqueous media [4].

The contribution of magnetization transfer effect can be included into the magnetization map for various tissues *in vivo*. Many experimentally measured M_s have been reported for human tissues such as brain grey/white matter, heart muscle, articular cartilage *etc.* [12,18], the magnetization map can be built with the additional measurement of R_{MT}. Based on R_{MT} value, the structures of paramagnetic ion chelates and the RF parameters for experiments can be optimized to minimize the influence of magnetization transfer. Thus, the magnetization map as the simulation tool can be used to design efficient paramagnetic labeling to target various anatomy/physiology in molecular imaging.

4.3. Theoretical magnetization profiles

Fig. 5 shows the residual z-magnetization profiles and three types of difference magnetization profiles for τ_R of 80 ps, 1500 ps and 3000 ps at 9.4 T. The same parameters as those in Fig. 4 are used except that the Gaussian lineshape function is used for R_{rfB}. The definition for the three types of difference magnetization profiles is provided in the Appendix A. These calculations are compared with those for the paramagnetic ion chelates in the aqueous media [4]. Fig. 5(A) shows the equilibrium residual z-magnetization profiles at $\tau = 500$ ms. This equilibrium status is refereed to the paramagnetic relaxation pathway; because the magnetization transfer pathway needs as long as a few seconds to reach the equilibrium. The magnetization profiles have two major changes in the gels: (1) the amplitude of magnetization profiles is reduced from ~100% to ~80% for $\Delta > 20$ kHz due to the magnetization transfer effect; (2) the dispersion at the low offset ($\Delta < 30$ kHz) is decreased due to the reduction of diffusion coefficient. The paramagnetic relaxation dominates the spin relaxations at the small offsets (large θ angle), where the reduction of dispersion in the residual z-magnetization profiles is expected for a smaller diffusion coefficient in gels [4].

Fig. 5(B) shows the type-1 difference magnetization profiles $\Delta M_{1,2-6}$, $\Delta M_{1,2-4}$ and $\Delta M_{1,4-6}$ generated from those shown in Fig. 5(A). The notations used in this paper are consistent the previous paper [4]. The subscript 1 denotes the type-1 difference magnetization profiles, 2–6 denotes the magnetization difference between ω_1 of 2 and 6 kHz, 2–4 denotes the magnetization difference between ω_1 of 2 and 4 kHz, and 4–6 denotes the magnetization difference between ω_1 of 4 and 6 kHz. These calculations are compared with those for the paramagnetic ion chelates in the aqueous media [4]. The type-1 difference magnetization profiles also have two changes in the gels: (1) the amplitude of the maximum reduces to ~0.4 in the gels instead of 0.5 in the solutions due to the magnetization transfer effect; (2) the distribution becomes narrower and the maxima shift to the lower frequency offset due to the reduction of diffusion coefficient, except for the τ_R of 80 ps. However, the features for characterizing the dynamics of paramagnetic ion chelates are preserved. Very similar to those in the aqueous media [4], the difference magnetization profiles shifts to the higher frequency offset and the maxima become broader as τ_R increases from 80 ps to 3000 ps. Thus, the type-1 difference magnetization profiles can be used to detect the dynamics of paramagnetic ion chelates in the presence of strong magnetization transfer effect.

Fig. 5(C) shows the type-2 difference magnetization profiles $\Delta M_{2,2-6}(\tau_i) = M_e(\tau_i, \theta_1) - M_e(\tau_i, \theta_3)$ generated from the transient magnetization profiles with RF amplitude of 2 and 6 kHz at pulse duration of 25 ms, 100 ms and 500 ms. The subscript 2 denotes the type-2 difference magnetization profiles and 2–6 denotes the magnetization difference between ω_1 of 2 and 6 kHz. These calculations are compared with those for the paramagnetic ion chelates in the aqueous media [4]. The changes in the type-2 difference magnetization profiles are somewhat different. The distribution is expected to become narrower for a reduced diffusion coefficient and the maximum is shifted to the lower frequency offset, except for the τ_R of 80 ps. However, the amplitude of the maximum decreases gradually as the pulse duration increases for all τ_R, from ~0.5 for $\tau = 25$ ms to ~0.4 for $\tau = 500$ ms. This is directly related to the magnetization transfer effect, because there is more magnetization loss due to the magnetization transfer effect at the longer pulse. This feature is different from that in the aqueous media, where the amplitude reaches a maximum between the short pulse and the long pulse. But the width and the frequency offset for the distribution are still correlated with the rotational correlation time in the gels. Thus, the type-2 difference magnetization profiles can be used for identifying the dynamics of paramagnetic ion chelates in the presence of magnetization transfer effect.

Fig. 5(D) shows the type-3 difference magnetization profiles $\Delta M_{3,\omega_i} = M_e(0.025, \theta_i) - M_e(0.5, \theta_i)$ generated by subtraction of $M_e(0.5, \theta)$ from $M_e(0.025, \theta)$ with RF amplitude of 2, 4 and 6 kHz. The subscript 3 denote the type-3 difference magnetization profile. These calculations are compared with those for the paramagnetic ion chelates in the aqueous media [4]. The type-3 difference magnetization profiles in the gels is seriously distorted by the magnetiza-

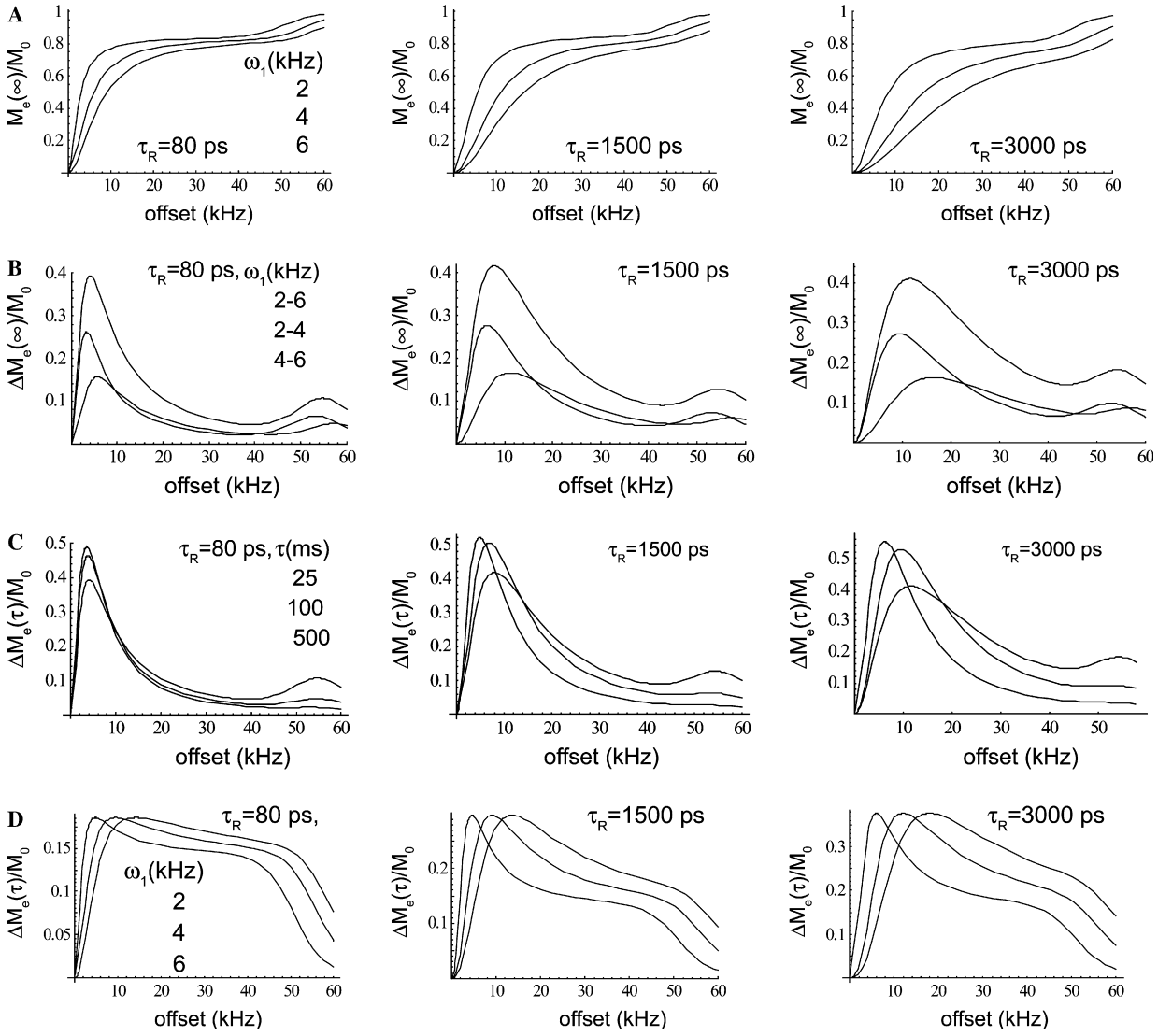

Fig. 5. Theoretically predicted various magnetization profiles for gadolinium chelates in cross-linked protein gels at 9.4 T. (A) Equilibrium residual z-magnetization profiles with RF amplitude of 2, 4 and 6 kHz, the profile with a larger dispersion corresponds to the higher RF amplitude. This equilibrium status is with respect to the paramagnetic relaxation pathway. (B) Type-1 difference magnetization profiles, $\Delta M_{1,2-6}$, $\Delta M_{1,2-4}$ and $\Delta M_{1,4-6}$. (C) Type-2 difference magnetization profiles $\Delta M_{2,2-6}(\tau_i)$ with $\tau_i = 25$, 100 ms and ∞, the maximum of the profiles shifts to higher offset as the pulse duration τ_i increases. (D) Type-3 difference magnetization profiles $\Delta M_{3,\omega_i}$ with $\omega_i = 2$, 4 and 6 kHz, the maximum of the profiles shifts to higher offset as the RF amplitude ω_i increases. Definition for the type of the magnetization profiles is shown in the Appendix A.

tion transfer at the large frequency offset ($\Delta > 25$ kHz). The distortion is much less for the τ_R of 3000 ps than that for the τ_R of 1500 ps. However, the maximum generated by the paramagnetic relaxation enhancement effect is preserved at the low frequency offset with amplitude depending on τ_R. Thus, the type-3 difference magnetization profiles still can be used to characterize the dynamics of paramagnetic ion chelates in the presence of magnetization transfer effect.

In summary, the presence of magnetization transfer effect does not affect the identifications of the rotational correlation time of paramagnetic ion chelates from the difference magnetization profiles. These calculations are for the paramagnetic ion chelates at 1 mM Gd(III) and a semi-rigid pool of 12 μs T_{2B} and 3.5 s^{-1} R_{MT}. In this case, the magnetization maps, the equilibrium residual z-magnetization profiles and three types of difference magnetization profiles can be correlated with the rotational correlation time τ_R directly. For most biological systems *in vivo*, the magnetization transfer is much weaker than the example shown here. Therefore, the dynamics of the paramagnetic agents is expected to be distinguishable by the pattern of the difference magnetization profiles. All above calculations are based on assumption of applying long TR. According to Eqs. (7), and (13), the magnetization transfer effect can be further suppressed by using short TR. In the discussion of experimental magnetization profiles presented in the following section, we will present the transient difference magnetization profiles obtained at short pulse duration τ and short TR, which permit the dynamics of

paramagnetic ion chelates in the presence of magnetization transfer effect to be extracted without the interference of the magnetization transfer effect.

4.4. Experimental magnetization profiles for Gd-DO3A in 10% BSA gels

Fig. 6(A) shows the residual z-magnetization profiles for Gd-DO3A in 10% cross-linked BSA gels with a 500 ms pulse at 9.4 T at 1 mM or 10 mM Gd(III). This experiment is used to confirm the proposed spin relaxation model. The cross-linking takes place between the –CHO on the glutaraldehyde and the primary amines on the protein [31], but no direct linkage is built between the chelates and the protein gels. Thus, Gd-DO3As are considered to be trapped in the protein gels. The residual z-magnetization profiles for 10 mM Gd(III) in the gels are very similar to those for the small τ_R in the aqueous media [4]. p_{Gd} is ~1 at this concentration for all frequency offsets and the influence of magnetization transfer completely disappears. This supports the competitive mechanism for the spin relaxation model shown in Section 2.1.

Fig. 6(B) shows the type-1 difference magnetization profiles $\Delta M_{1,2-6}$, $\Delta M_{1,2-4}$ and $\Delta M_{1,4-6}$ generated from those shown in Fig. 6(A). The difference magnetization profiles for 10 mM Gd-DO3A are very similar to those for the small τ_R in the aqueous media [4]. The amplitude for the maximum is ~0.38 in the gels, which is smaller than that in aqueous media (~0.5). As the concentration of Gd-DO3A decreases to 1 mM, the maxima are located at nearly the same frequency offset except for the wider distributions. Thus, these frequency offsets are the inherent characteristics for identifying the dynamics of paramagnetic ion chelates in the presence of magnetization transfer effect regardless the contribution fraction p_{Gd}.

Note that Gd-DO3A is a small chelate, its small τ_R does not generate notable relaxation enhancement in the off-resonance rotating frame, $R_{1\rho,Gd}(\theta)/R_1 \sim 1$. For the paramagnetic chelates with large τ_R and significant enhancement effect ($R_{1\rho,Gd}(\theta)/R_1 \gg 1$), the Gd(III) concentration can be lower than 1 mM. The increase of hydration number q also helps to increase the relaxation rate constant ratio $R_{1\rho,Gd}(\theta)/R_{MT}$. Thus, this method is expected to be applicable *in vivo*.

4.5. Experimental magnetization profiles for $(Gd\text{-}DTPA)_n$-macromolecule in 7% BSA gels

Fig. 7(A) shows the residual z-magnetization profiles obtained at 9.4 T for Dextran attached Gd-DTPA and Dendrimer attached GD-DTPA at 1 mM Gd(III) in 7% cross-linked BSA gels. These paramagnetic ion chelates are the same as those used in the aqueous media [3,4]. The averaged molecular formula are $(Gd\text{-}DTPA)_8$-Dextran and $(Gd\text{-}DTPA\text{-}SCN\text{-}Bz)_{41}$-PAMAM-g5, respectively. The two chelates have quite different τ_R as demonstrated by their difference magnetization profiles in the aqueous media [4]. Thus, these chelates are chosen to demonstrate the correlation of the τ_R with various magnetization profiles in the gels. Dextran does not react with the cross-linking agent

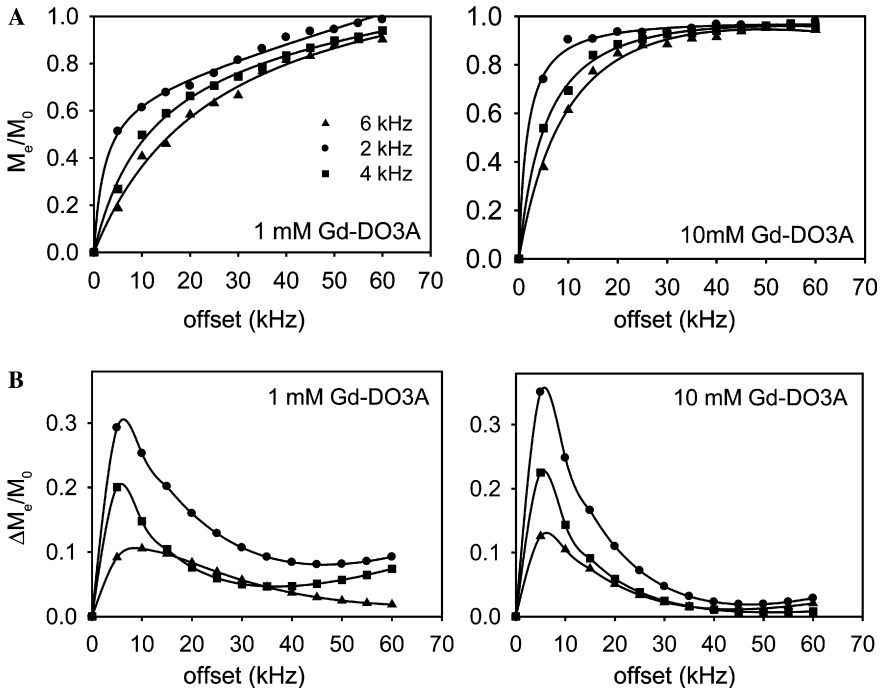

Fig. 6. Experimentally measured various magnetization profiles for aqueous Gd-DO3A at 1 or 10 mM Gd(III) in 10% cross-links BSA gels at 9.4 T. (A) Residual z-magnetization profiles obtained with pulse duration of 500 ms and RF amplitude of 2, 4 and 6 kHz. (B) Type-1 difference magnetization profiles, $\Delta M_{1,2-6}$, $\Delta M_{1,2-4}$ and $\Delta M_{1,4-6}$.

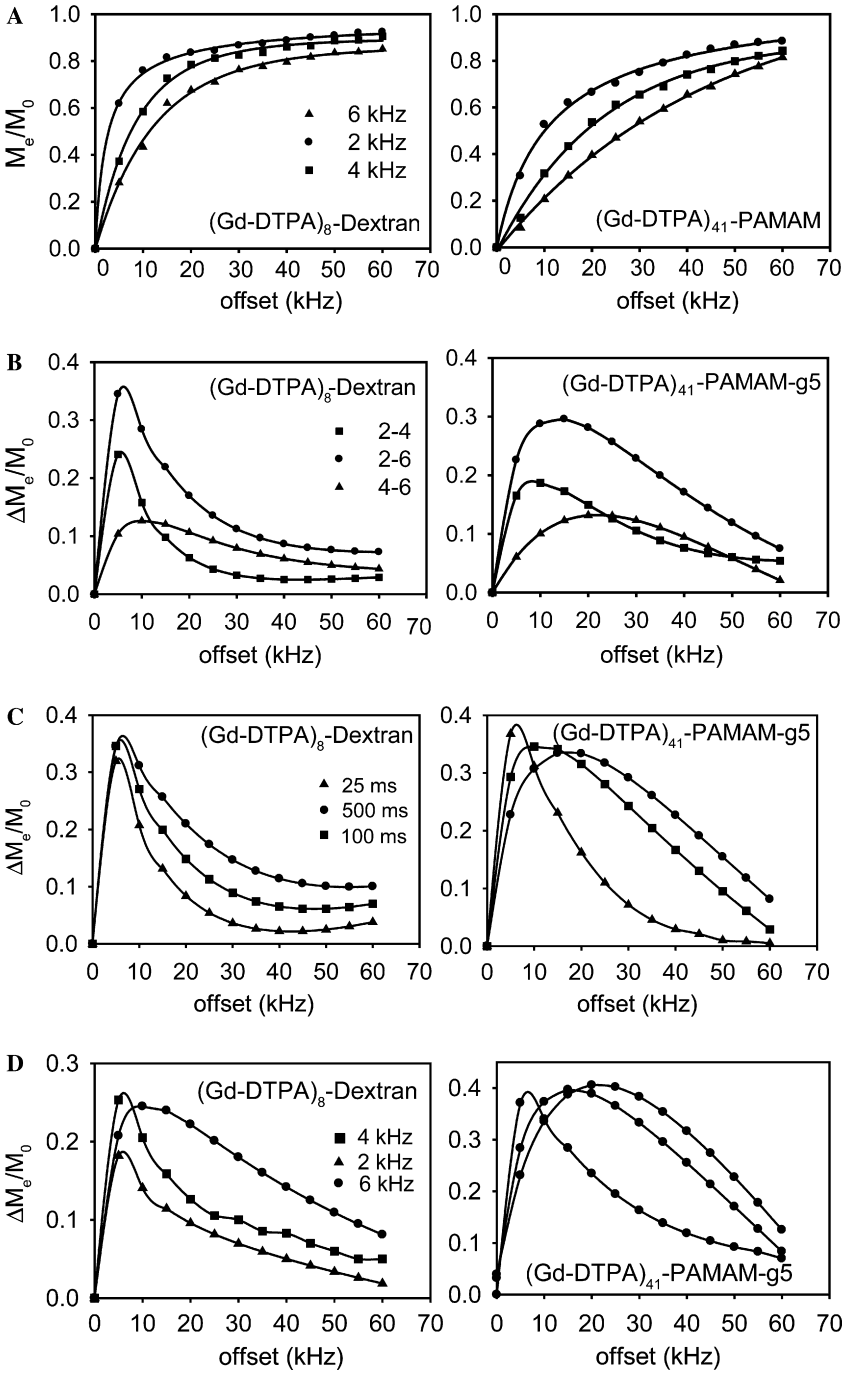

Fig. 7. Experimentally measured various magnetization profiles for aqueous (Gd-DTPA)*n*-macromolecules at 1 mM Gd(III) in 7% cross-linked BSA gels at 9.4 T. (A) Residual *z*-magnetization profiles obtained with pulse duration of 500 ms and RF amplitude of 2, 4 and 6 kHz. (B) Type-1 difference magnetization profiles, $\Delta M_{1,2-6}$, $\Delta M_{1,2-4}$ and $\Delta M_{1,4-6}$. (C) Type-2 difference magnetization profiles $\Delta M_{2,2-6}(\tau_i)$ with $\tau_i = 25$, 100 ms and ∞. (D) Type-3 difference magnetization profiles $\Delta M_{3,\omega_i}$ with $\omega_1 = 2$, 4 and 6 kHz.

glutaraldehyde. Dendrimer have many bulky chelates that prevents the effective cross-linkage. These paramagnetic ion chelates are more likely to be trapped in the gels instead of binding to the immobilized proteins. Comparing with the aqueous media, $R^{IS}_{1\rho,Gd}$ increases due to the increase of rotation correlation time τ_R in the gels; $R^{OS}_{1\rho,Gd}$, $R^{OS}_{1,Gd}$ also increase because the decrease of diffusion coefficient D in the gels. The increase of τ_R will increase the relaxation enhancement efficiency; while the decrease in D will reduce the relaxation enhancement efficiency. If the effect of τ_R is larger than the effect of D, the dynamic range of magnetization map will increase. This change will be reflected on the residual *z*-magnetization profiles and the difference magnetization profiles. For the residual *z*-magnetization profiles shown here, it is consistent with the theoretical predictions shown in Fig. 5(A) that the amplitude of the

magnetization decreases to ~0.85 accompanying with slight reduction in the dispersion. The dispersion of these residual z-magnetization profiles suggests that the rotational correlation time is larger for $(Gd\text{-}DTPA\text{-}SCN\text{-}Bz)_{41}$-PAMAM-g5 than that for $(Gd\text{-}DTPA)_8$-Dextran, which is consistent with that in the aqueous media [4].

Fig. 7(B) shows the type-1 difference magnetization profiles generated from those shown in Fig. 7(A). These experimental data in the gels are used to compare with those in the aqueous media [4]. For both paramagnetic ion chelates, the amplitude of the maxima is reduced to 0.3–0.35 in the gels instead of 0.45–0.5 in the solutions because the magnetization transfer effect. This is consistent with the above theoretical predictions. The distributions are much wider and the maxima are located at higher frequency offset in the gels. These alterations are more apparent for PAMAM-g5 than that for Dextran, which suggests the substantial increase of τ_R for both paramagnetic ion chelates. When we compare the features for the same τ_R in different media in the theoretical calculations, the only parameter changed is the diffusion coefficient D. However, when we compare the experimental results for the same paramagnetic ion chelates in the gels, both τ_R and D are altered. Comparing with the theoretical calculations shown in Fig. 5(B), τ_R is ~1000 ps for Dextran attached chelates and ~3000 ps for PAMAM-g5 attached chelates in the gel media, which are much larger than those in the aqueous media. However, the maxima in the gels remain at nearly the same frequency offset as that in the solutions [4], which suggests that the increase of τ_R has larger effect on $R_{1\rho,Gd}(\theta)/R_1$ than the decrease of D.

Fig. 7(C) shows the type-2 difference magnetization profiles $\Delta M_{2,2\text{–}6}(\tau_i)$ for $(Gd\text{-}DTPA)_8$-Dextran and $(Gd\text{-}DTPA\text{-}SCN\text{-}Bz)_{41}$-PAMAM-g5 at 1 mM Gd(III) in 7% BSA gels at 9.4 T with pulse duration of 0.025 s, 0.1 s and 0.5 s. The amplitude of the maximum decreases as τ increases because the magnetization transfer effect, which is consistent with theoretical prediction shown in Fig. 5(C). The distributions are much wider and the maxima are located at higher frequency offset in the gels than those in the solutions, suggesting that the increase of τ_R has larger effect on $R_{1\rho,Gd}(\theta)/R_1$ than the decrease of D. The maxima for PAMAM-g5 appears much broader at long pulses than the theoretical predictions, partly due to that the calculations are not completely fitted with the experimental data at the high frequency offset ($\Delta > 30$ kHz). However, this error does not affect the identification of the rotational correlation time via the maxima at the low offset. The rotational correlation times extracted from the type-2 difference magnetization profiles are consistent with that from the type-1, which is ~1000 ps for Dextran attached chelates and ~3000 ps for PAMAM-g5 attached chelates.

Fig. 7(D) shows the type-3 difference magnetization profiles $\Delta M_{3,\omega_i} = M_e(0.025, \theta_i) - M_e(\infty, \theta_i)$ for $(Gd\text{-}DTPA)_8$-Dextran and $(Gd\text{-}DTPA\text{-}SCN\text{-}Bz)_{41}$-PAMAM-g5 at 1 mM Gd(III) in 7% BSA gels at 9.4 T with RF amplitude of 2, 4 and 6 kHz. For the Dextran attached chelates, the distributions in the gel media are very similar to that in the aqueous media [4]. But the amplitude for the maxima is ~0.25 in the gels, which is higher than that in the solutions (~0.12). For the PAMAM-g5 attached chelates, the distributions are much broader than those in the solutions. The maxima shift to the high frequency offset with the amplitude ~0.39 in the gels, which is higher than that in the solutions (~0.31). Since the amplitude of the maxima is proportional to the rotational correlation time, the increase in the amplitude of maxima for both paramagnetic ion chelates suggests that their τ_R increases substantially in the gels. Note that the theoretical predictions are quite different from the experimental data at the large frequency offsets, as shown by comparing Fig. 5(D) with Fig. 7(D). The calculated profiles have much higher intensity in this region; while the experimental profiles are actually very similar to those in the aqueous media. All these differences are located at the large frequency offset, which should not affect the identification of the dynamics via the maxima located at the low frequency offset. The experimental data from the type-3 difference magnetization profiles suggest that τ_R is ~1000 ps for the Dextran attached chelates and ~3000 ps for the PAMAM-g5 attached chelates.

In agreed with the numerical simulations, all three types of experimental difference magnetization profiles demonstrate the dynamics difference for the macromolecules conjugated chelates in the gels. This suggests that any of these difference magnetization profiles can be used to efficiently differentiate the dynamics of paramagnetic ion chelates in the presence of magnetization transfer effect.

4.6. Theoretical and experimental magnetization profiles at short τ and TR

Fig. 8 shows transient residual z-magnetization profiles for $(Gd\text{-}DTPA)_8$-Dextran and $(Gd\text{-}DTPA\text{-}SCN\text{-}Bz)_{41}$-PAMAM-g5 at 1 mM Gd(III) in 7% BSA gels at 9.4 T. The residual z-magnetization profiles for 7% BSA gels alone are also shown in Fig. 8 as a reference. This experiment compares the magnetizations obtained with a set of short τ and TR in the limit of $TR \gg \tau$. RF conditions can be defined from this study to obtain a new type of difference magnetization $\Delta M(\tau, TR)$ that is solely contributed from the paramagnetic relaxation pathway. This $\Delta M(\tau, TR)$ must meet two criteria: (1) it is predominated by the paramagnetic relaxation for the paramagnetic agents/gels compartment (>95%); (2) it is negligible for the gels compartment. Based on the theoretical discussions in Section 2.4, a short TR is expected to saturate the spins associated with the magnetization transfer pathway but not those spins associated with the paramagnetic relaxation pathway; and a short τ allows sufficient paramagnetic relaxation but negligible magnetization transfer.

For the PAMAM-g5 attached chelates in the gels, the residual z-magnetization profiles obtained with the pulse duration of 25 ms and 100 ms are identical for 1 s TR and 20 s TR at the frequency offset $\Delta < 35$ kHz. This result

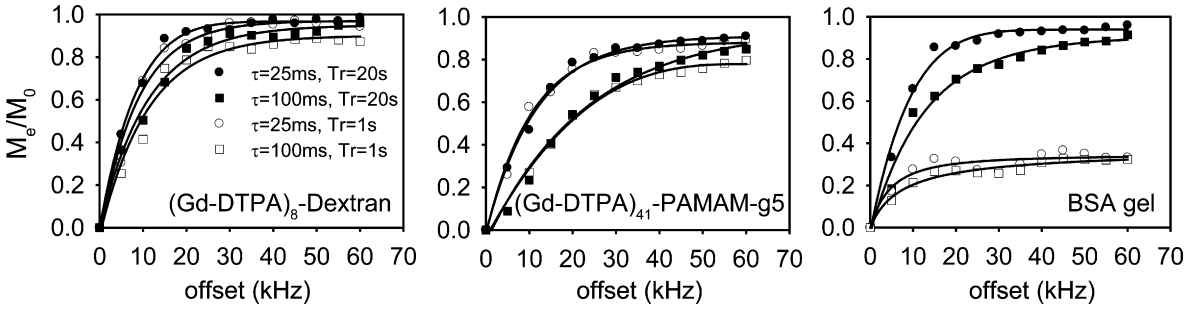

Fig. 8. Experimentally measured magnetization profiles for aqueous (Gd-DTPA)n-macromolecules at 1 mM Gd(III) in 7% cross-linked BSA gels at 9.4 T. The experiments were carried out at short pulse duration τ and short TR with $\omega_1 = 6$ kHz. The left and center panels are for the protein gels with paramagnetic ion chelates, the right panel is for the protein gels alone.

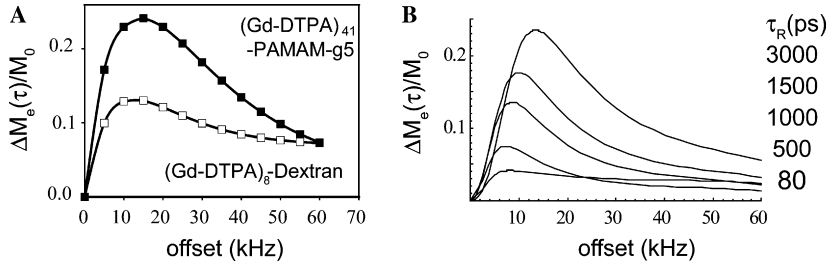

Fig. 9. Experimentally measured (A) and theoretically predicted (B) difference magnetization profiles for aqueous (Gd-DTPA)n-macromolecules at 1 mM Gd(III) in 7% cross-linked BSA gels at 9.4 T. The experimental data were generated from Fig. 8. Molecular parameters are discussed in the text.

suggests that the total spin relaxation at 1 s TR is predominated by the paramagnetic relaxation pathway. τ and TR in this experiment are selected arbitrarily, only for the purpose of demonstrating the trend. The spins that are primarily relaxed by the magnetization transfer effect are saturated at $\Delta > 35$ kHz. The magnetization for 1 s TR begins to decrease and more decrement occurs at the longer pulse. The Dextran attached chelates have smaller paramagnetic relaxation rate constant $R_{1\rho,\mathrm{Gd}}(\theta)$ than the PAMAM-g5 attached chelates, the decrement caused by the magnetization transfer effect takes place at much lower offset. However, the decrement at $\tau = 25$ ms is nearly the same as that at $\tau = 100$ ms. Their difference magnetization is affected. The residual z-magnetizations for the BSA gels are very different at 1 s TR and 20 s TR. The difference magnetization obtained at the two pulse durations is ~0.2 for 20 s TR, which is large enough in comparing with that with the paramagnetic agents; but it reduces to than 0.03 for 1 s TR, which is negligible in comparing with that with the paramagnetic agents. Thus, short TR will suppress the signal originated from the magnetization transfer effect so that the paramagnetic relaxation pathway becomes dominant.

Fig. 9(A) shows the experimental difference magnetization profiles generated from those shown in the left panel and the middle panel of Fig. 8. This type of difference magnetization profiles has a broad distribution. The amplitude and the frequency offset for the maxima are a function of the rotational correlation time τ_R. For the PAMAM-g5 attached chelates, the amplitude is 0.25 and the frequency offset is 15 kHz. The Dextran attached chelates have a smaller τ_R, the amplitude reduces to 0.14 and the frequency offset shifts down to 10 kHz. The dependence on τ_R is further confirmed by the theoretical calculations shown in Fig. 9(B). As τ_R increases, the maximum shifts to the higher frequency offset with increased amplitude. The simulations suggest that τ_R is ~1000 ps for the Dextran attached chelates and ~3000 ps for the dendrimer attached chelates, which is consistent with the results discussed in Section 4.5. This type of difference magnetization profiles has many advantages for the *in vivo* applications: (1) the short pulse duration reduces the RF power depositions substantially; (2) the amplitude and frequency offset of the maxima can be used to define τ_R accurately; (3) the magnitude has little contribution from the magnetization transfer effect for the compartments with the paramagnetic agents; and (4) the magnitude is negligible for the compartments without the paramagnetic agents.

5. Conclusions

A theoretical model is established for the spin relaxations of water protons in the presence of paramagnetic ion chelates and magnetization transfer effect in off-resonance rotating frame. Based on this spin relaxation model, the total residual z-magnetization is the sum of the contributions from two relaxation pathways: the paramagnetic relaxation and the magnetization transfer. The contribution fraction for each pathway is determined by the competition of the two pathways, in which the paramagnetic relaxation pathway can dominate the total relaxation via paramagnetic relaxation enhancement effect. The model is

further validated with the experimental measurement for Gd-DO3A at 1 and 10 mM Gd(III) in 10% BSA gels. Using this model, the effect of magnetization transfer on the total residual z-magnetization are quantified in the context of the magnetization map and various difference magnetization profiles, which have been shown to be the powerful tool in evaluating the rotational correlation time of paramagnetic ion chelates in aqueous media [4]. This permits us to apply the techniques established for the aqueous media to the gel media, including the use of the magnetization map as a simulation tool to select RF parameters for experiments and the difference magnetization profiles to generate standards for identifying the dynamics of paramagnetic ion chelates. In the similar way as in the previous paper [4], the magnetization map and the difference of magnetization profiles are correlated with the correlation time τ_R of Gd-DTPA through numerical simulations, which are further validated by the experimental data for the macromolecule conjugated Gd-DTPA in 7% cross-linked BSA gel. These studies confirm that the rotational correlation time for paramagnetic ion chelates can be determined even in the presence of magnetization transfer effect. This spin relaxation model also provides guidance for editing the relaxation contributions to the signal, such as using short pulse duration to reduce the amount of magnetization transfer and short TR to saturate the spins involved in the magnetization transfer pathway. Along this line, a new type of difference magnetization profiles has been explored with the theoretical simulations and experimental measurements. Like in the aqueous media, this method not only can determine the dynamics for the T_1-type paramagnetic agents but also can evaluate the relaxation enhancement efficiency for the T_2-type paramagnetic agents in the presence of magnetization transfer effect [4]. The inclusion of the magnetization transfer effect allows us to use the magnetization map as a simulation tool to design efficient paramagnetic labeling targeting at specific tissues, to design experiments running at low RF power depositions, and to optimize the sensitivity for detecting paramagnetic labeling. Thus, the presented method will be a very useful tool for *in vivo* applications such as molecular imaging via paramagnetic labeling.

Acknowledgment

This work was supported by grant to H.Z. from the National Institutes of Health (EB02912).

Appendix A

We provide here the rotating frame spin–lattice relaxation rate constants for the inner shell water $R_{1\rho}^{IS}(\theta)$ and for the outer shell of water $R_{1\rho}^{OS}(\theta)$ that are used in Eq. (4). The detailed derivations for these parameters have been originally described in the previous paper [3].

The rotating frame spin–lattice relaxation rate constant for inner shell water is as follows:

$$R_{1\rho}^{IS}(\theta)=\frac{P_M q}{1/R_{1\rho,d}(\theta)+\tau_m} \tag{A.1}$$

where P_m is the molar fraction of metal ion, q is the number of water molecular bound per metal ion, τ_m is the residual life time of the bound water. $R_{1\rho,d}(\theta)$ is the rotating frame spin lattice relaxation rate constant caused by electron-dipolar coupling interaction and is expressed as follows:

$$\begin{aligned}R_{1\rho,d}(\theta)=K\{&2\sin^2\theta J(\omega_e)+\sin^4(\theta/2)J(\omega_S-\omega_H+\omega_e)\\&+\cos^4(\theta/2)J(\omega_S-\omega_H-\omega_e)+3\cos^4(\theta/2)J(\omega_H+\omega_e)\\&+3\sin^4(\theta/2)J(\omega_H-\omega_e)+3/2\sin^2\theta(J(\omega_S+\omega_e)\\&+J(\omega_S-\omega_e))+6\cos^4(\theta/2)J(\omega_S+\omega_H+\omega_e)\\&+6\sin^4(\theta/2)J(\omega_S+\omega_H-\omega_e)\}.\end{aligned} \tag{A.2}$$

At the high magnetic field, $\omega_S \gg \omega_H \gg \omega_e$, $R_{1\rho,d}(\theta)$ can be simplified as

$$R_{1\rho,d}(\theta)\sim K\{2f_1(\theta)J(\omega_e)+3f_2(\theta)J(\omega_H)\} \tag{A.3}$$

In this formalism,

$$K=\frac{2}{15}\frac{\gamma_H^2\gamma_S^2\hbar^2S(S+1)}{r^6}$$

$$f_1(\theta)=\sin^2(\theta)$$

$$f_2(\theta)=\sin^4(\theta/2)+\cos^4(\theta/2)$$

$$(\omega)=\frac{\tau_c}{1+\omega^2\tau_c^2}$$

$$\tau_c^{-1}=\tau_R^{-1}+\tau_m^{-1}+T_{1e}^{-1}$$

$$T_{1e}^{-1}=\frac{1}{5\tau_{S0}}\left[\frac{1}{1+\omega_S^2\tau_v^2}+\frac{4}{1+4\omega_S^2\tau_v^2}\right]$$

where θ is the angle for the effective field, τ_v is the correlation time characterizing the fluctuation of the zero field splitting (ZFS) and τ_{S0} is related to ZFS constant B as $\tau_{S0}=\tau_v/5B$. For the macromolecule conjugated paramagnetic chelates, τ_m is the residual time of structural water, T_{1e} is electronic relaxation time. τ_R is the rotational correlation time, which is a sum of contributions from internal

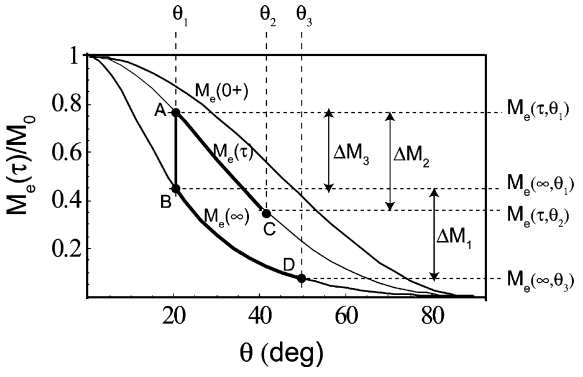

Fig. A1.

reorientation motion (τ_i) and global tumbling motion (τ_g) and $\tau_R^{-1} = \tau_i^{-1} + \tau_g^{-1}$.

The rotating frame spin lattice relaxation rate constant for the outer shell $R_{1\rho}^{OS}(\theta)$ is expressed as,

$$R_{1\rho}^{OS}(\theta) = K'\{2f_1(\theta)(1+\alpha B_S^2(x))J_{1OS}(\omega_e) + 3f_2(\theta) \times [(1+\alpha)B_S^2(x)J_{1OS}(\omega_H, \tau_D, T_{1e} \to \infty) + (1 - B_S^2(x))J_{1OS}(\omega_H, \tau_D, T_{1e})]\} \quad (A.4)$$

with

$$K' = \frac{32\pi}{405}\hbar^2\gamma_H^2\gamma_S^2 S(S+1)\frac{N_A}{1000}\left(\frac{C}{dD}\right)$$

$$J_{1OS}(\omega_H, \tau_D, T_{1e}) = \mathrm{Re}\Big(\{1 + (1/4)(i\omega\tau_D + \tau_D/T_{1e})\} / \Big\{1 + (i\omega\tau_D + \tau_D/T_{1e})^{1/2} + (4/9) \times (i\omega\tau_D + \tau_D/T_{1e}) + (1/9)(i\omega\tau_D + \tau_D/T_{1e})^{3/2}\Big\}\Big)$$

$$\tau_D = d^2/D$$

$$B_S(x) = \left(\frac{2S+1}{2S}\right)\coth\left[\left(\frac{2S+1}{2S}\right)x\right] - \left(\frac{1}{2S}\right)\coth\left[\frac{x}{2S}\right]$$

where $x = \mu B_0/RT$, $\alpha = (2S-1)/(S+1)$, μ is the magnetic moment of metal ion, $\mu = \gamma_S\hbar S$, N_A is the number of metal ion per cubic centimeter, d is the distance of closet approach of the water to the metal complex, τ_D is the relative translation diffusion time, $\tau_D = d^2/3(D_H + D_S)$, D_H and D_S are the diffusion coefficients of water and metal ion.

Three types of difference magnetization profiles generated from the magnetization map are shown in Fig. A1 in this appendix section [4]. In the magnetization map, $M_e(0_+)$ defines the upper limit and $M_e(\infty)$ defines the lower limit. A, B, C and D are the labels for the magnetization $M_e(\tau,\theta)$ selected arbitrarily, where A denotes for $M_e(\tau,\theta_1)$, B denotes for $M_e(\infty,\theta_1)$, C denotes for $M_e(\tau,\theta_2)$ and D denotes for $M_e(\infty,\theta_3)$. The dark black lines represent the path for generating the difference magnetization. Three types of difference magnetization profiles can be generated: type-1 is defined by the path BD, $\Delta M_1 = M_e(\infty,\theta_1) - M_e(\infty,\theta_3)$; type-2 is defined by the path AC, $\Delta M_2 = M_e(\tau,\theta_1) - M_e(\tau,\theta_2)$; and type-3 is defined by the path AB, $\Delta M_3 = M_e(\tau,\theta_1) - M_e(\infty,\theta_1)$.

References

[1] S.H. Koenig, R.D. Brown III, Relaxometry of magnetic resonance imaging contrast agents, Magn. Reson. Annu. (1987) 263–286.

[2] S.H. Koenig, R.D. Brown III, Field-cycling relaxometry of protein solutions and tissue: implications for MRI, Prog. NMR spectrosc. 22 (1990) 487–567.

[3] H. Zhang, Y. Xie, Efficiency of paramagnetic relaxation enhancement in off-resonance rotating frame, J. Magn. Reson. 181 (2006) 212–222.

[4] H. Zhang, Y. Xie, Dynamics of paramagnetic agents by off-resonance rotating frame technique, J. Magn. Reson. 183 (2006) 213–227.

[5] P.J. Keller, W.W. Hunter Jr., P. Schmalbrock, Multisection fat-water imaging with chemical shift selective presaturation, Radiology 164 (1987) 539–541.

[6] S.D. Wolff, R.S. Balaban, Magnetization transfer contrast (MTC) and tissue water proton relaxation in vivo, Magn. Reson. Med. 10 (1989) 135–144.

[7] T.L. James, G.B. Matson, I.D. Kuntz, R.W. Fisher, Rotating frame spin–lattice relaxation in the presence of an off-resonance radio frequency field. Investigation of intermediate molecular motions, J. Magn. Reson. 28 (1977) 417–426.

[8] T.L. James, G.B. Matson, I.D. Kuntz, Protein rotational correlation times determined in aqueous solution by carbon-13 rotating frame spin–lattice relaxation in the presence of an off-resonance radiofrequency field, J. Am. Chem. Soc. 100 (1978) 3590–3594.

[9] T. Schleich, C.F. Morgan, G.H. Caines, Protein rotational correlation times by carbon-13 rotating-frame spin–lattice relaxation in presence of off-resonance radiofrequency field, Methods Enzymol. 176 (1989) 386–418.

[10] C.F. Morgan, T. Schleich, G.B. Caines, Assessment of protein reorientational diffusion in solution by ^{13}C off-resonance rotating frame spin–lattice relaxation: effect of polydispersity, Biopolymers 29 (1990) 501–507.

[11] J.M. Rydzewski, T. Schleich, Deuterium off-resonance rotating frame spin–lattice relaxation of macromolecular bound ligands, Biophys. J. 70 (1996) 1472–1484.

[12] R.S. Balaban, T.L. Ceckler, Magnetization transfer contrast in magnetic resonance imaging, Magn. Reson. Quart. 8 (1992) 116–137.

[13] R.M. Henkelman, G.J. Stanisz, S.J. Graham, Magnetization transfer in MRI: a review, NMR Biomed. 14 (2001) 57–64.

[14] D. Brooks, K. Kuwata, T. Schleich, Determination of proton magnetization transfer rate constants in heterogeneous biological systems, Magn. Reson. Med. 31 (1994) 331–336.

[15] J.J. Tessier, N. Dillon, T.A. Carpenter, L.D. Hall, Interpretation of magnetization transfer and proton cross-relaxation spectra of biological tissues, J. Magn. Reson. B107A (1995) 138–144.

[16] R.M. Henkelman, X. Huang, Q.-S. Xiang, G.J. Stanisz, S.D. Swanson, M.J. Bronskill, Quantitative interpretation of magnetization transfer, Magn. Reson. Med. 29 (1993) 759–766.

[17] C. Morrison, R. Mark Henkelman, A model for magnetization transfer in tissues, Magn. Reson. Med. 33 (1995) 475–482.

[18] J.G. Li, S.J. Graham, R.M. Henkelman, A flexible magnetization transfer lineshape derived from tissue experimental data, Magn. Reson. Med. 37 (1997) 866–870.

[19] J. Grad, D. Mendelson, F. Hyder, R.G. Bryant, Direct measurements of longitudinal relaxation and magnetization transfer in heterogeneous systems, J. Magn. Reson. 86 (1990) 416–419.

[20] J. Eng, T.L. Ceckler, R.S. Balaban, Quantitative ^1H magnetization transfer imaging *in vivo*, Magn. Reson. Med. 17 (1991) 304–314.

[21] H.N. Yeung, Transient responses of a heterogeneous spin system to binomial pulse saturation, J. Magn. Reson. A 102 (1993) 8–15.

[22] H.N. Yeung, S.D. Swanson, Transient decay of longitudinal magnetization in heterogeneous spin systems under selective saturation, Magn. Reson. Med. 99 (1992) 466–479.

[23] G.B. Pike, Pulse magnetization transfer contrast in gradient echo imaging: a two-pool analytic description of signal response, Magn. Reson. Med. 36 (1996) 95–103.

[24] J.G. Sled, G.B. Pike, Quantitative imaging of magnetization transfer in spoiled gradient echo MRI, J. Magn. Reson. 145 (2000) 24–36.

[25] W.B. Pierce, S.E. Harms, D.P. Flamig, R.H. Griffey, W.P. Evans, J.E. Hagans, Three dimensional gadolinium-enhanced MR imaging of the breast: pulse sequence with fat suppression and magnetization transfer contrast, Radiology 181 (1991) 757–763.

[26] H.J. Tan, R.E. Sepponen, M.J. Lipton, T. Kuusela, Synergistic enhancement of MRI with Gd-DTPA and magnetization transfer, J. Comput. Assist. Tomogr. 16 (1992) 16–24.

[27] R.M. Henkelman, G.J. Stanisz, N. Menezes, D. Burstein, Can MTR be used to access cartilage in the presence of Gd-DTPA^{2-}? Magn. Reson. Med. 48 (2002) 1081–1084.

[28] T. Kurki, M. Komu, Spin-lattice relaxation and magnetization transfer in intracranial tumors in vivo: effects of Gd-DTPA on relaxation parameters, Magn. Reson. Imaging 13 (1995) 379–385.

[29] I. Bertini, C. Luchinat, G. Parigi, G. Quacquarini, P. Marzola, F.M. Cavagna, Off-resonance experiments and contrast agents to improve magnetic resonance imaging, Magn. Reson. Med. 39 (1998) 124–131.

[30] S.H. Koenig, R.D. Brown III, R. Ugolini, Magnetization transfer in cross-linked bovine serum albumin solutions at 200 MHz: a model for tissue, Magn. Reson. Med. 29 (1993) 311–316.
[31] K. Peters, F.M. Richards, Chemical cross-linking: reagents and problems in studies of membrane structure, Ann. Rev. Biochem. 46 (1977) 523–551.
[32] B.J. Balcom, T.J. Lees, A.R. Sharp, N.S. Kulkarni, G.S. Wagner, Diffusion in Fe(II/III) radiation dosimetry gels measured by magnetic resonance imaging, Phys. Med. Biol. 40 (1995) 1665–1676.
[33] T.V. Pedersen, D.R. Olsen, A. Skretting, Measurement of the ferric diffusion coefficient in agarose and gelatine gels by utilization of the evolution of radiation induced edge as reflected in relaxation rate images, Phys. Med. Biol. 42 (1997) 1575–1585.
[34] S.H. Koenig, R.D. Brown III, R. Ugolini, Magnetization transfer in cross-linked bovine serum albumin solutions at 200 MHz: a model for tissue, Magn. Reson. Med. 29 (1993) 311–315.
[35] H.I. Mäkelä, M.I. Kettunen, O.H.J. Gröhn, R.A. Kauppinen, Quantitative $T_{1\rho}$ and magnetization transfer magnetic resonance imaging of acute cerebral ischemia in the rat, J. Cereb. Blood Flow Met. 22 (2002) 547–558.
[36] J. Zhou, J.-F. Payen, A.A. Wilson, R.J. Traystman, P.C. van Zijl, Using the amide proton signals of intracellular proteins and peptides to detect pH effects in MRI, Nat. Med. 9 (2003) 1085–1090.